

## DETECTION OF EXTREMELY BROAD WATER EMISSION FROM THE MOLECULAR CLOUD INTERACTING SUPERNOVA REMNANT G349.7+0.2

J. RHO<sup>1, 2</sup>, J. W. HEWITT<sup>3</sup>, A. BOOGERT<sup>4</sup>, M. KAUFMAN<sup>5</sup> AND A. GUSDORF<sup>6</sup>

*Accepted for the publication in ApJ, August, 2015*

### ABSTRACT

We performed *Herschel* HIFI, PACS and SPIRE observations towards the molecular cloud interacting supernova remnant G349.7+0.2. An extremely broad emission line was detected at 557 GHz from the ground state transition  $1_{10}$ - $1_{01}$  of ortho-water. This water line can be separated into three velocity components with widths of 144, 27 and 4 km s<sup>-1</sup>. The 144 km s<sup>-1</sup> component is the broadest water line detected to date in the literature. This extremely broad line width shows importance of probing shock dynamics. PACS observations revealed 3 additional ortho-water lines, as well as numerous high-J carbon monoxide (CO) lines. No para-water lines were detected. The extremely broad water line is indicative of a high velocity shock, which is supported by the observed CO rotational diagram that was reproduced with a J-shock model with a density of 10<sup>4</sup> cm<sup>-3</sup> and a shock velocity of 80 km s<sup>-1</sup>. Two far-infrared fine-structure lines, [O I] at 145 micron and [C II] line at 157 micron, are also consistent with the high velocity J-shock model. The extremely broad water line could be simply from short-lived molecules that have not been destroyed in high velocity J-shocks; however, it may be from more complicated geometry such as high-velocity water bullets or a shell expanding in high velocity. We estimate the CO and H<sub>2</sub>O densities, column densities, and temperatures by comparison with RADEX and detailed shock models.

*Subject headings:* ISM:molecules - ISM:supernova remnants - ISM:individual objects (G349.7+0.2) - shock waves

### 1. INTRODUCTION

Water is the basic building block of life and is often used as a diagnostic for forms of life on planets (Archer et al. 2014). Water may be formed by ion-neutral reactions in cold gas, through grain surface reactions or neutral-neutral reactions at higher temperatures (e.g. Hollenbach et al. 2009). High water abundances are possible behind shocks either due to chemical reactions or due to sputtering of ice mantles. One of the most important post-shock reactions is  $O + H_2 \Rightarrow OH + H$  followed by  $OH + H_2 \Rightarrow H_2O + H$ , which rapidly forms H<sub>2</sub>O in the gas phase.

Theoretical models predict that in shocks water is a powerful coolant, second in importance only to H<sub>2</sub> (Kaufman & Neufeld 1996; Flower & Pineau Des Forêts 2010). However, recent observations suggest that H<sub>2</sub>O may be less important as a coolant and the water abundance may be reduced in shocks (Karska et al 2014; Santangelo et al 2014). On the other hand, Neufeld et al. (2014) find that H<sub>2</sub>O formation is as efficient as expected, driving all O into H<sub>2</sub>O, as soon as shock speeds are high enough to convert

O-bearing ices to the gas phase. Therefore, the study of water in shocks is important to resolve this controversy.

Water is widely detected in protostellar outflows (e.g. van Dishoeck et al. 2011, and references therein). In contrast, to date, water has been detected from only three supernova remnants, namely 3C391, IC 443 and W28 (Reach & Rho 1998; Snell et al. 2005; Neufeld et al. 2014). Of these, only IC 443 exhibited broad water lines, with line widths in excess of 30 km s<sup>-1</sup> (FWHM). Broad CO lines (~20-40 km s<sup>-1</sup>) have been detected from a handful of SNRs including 3C391 (Reach & Rho 1998), IC443 (van Dishoeck et al. 1993), W28 and W44 (Reach, Rho & Jarrett 2005; Gusdorf et al. 2012; Anderl et al. 2014). Despite the increasing number of SNRs that are known to be interacting with molecular clouds, attempts to model the observed shock diagnostics revealed in these spectra have mainly indicated the complexity of interstellar shocks (e.g. Hewitt et al. 2009, H09 hereafter).

In this letter, we present *Herschel* HIFI spectra of ground-state emission from ortho-H<sub>2</sub>O; this line emission, which includes extremely broad velocity components, is compared with additional H<sub>2</sub>O lines, CO lines, and fine structure lines of [O I] and [C II], all detected with the *Herschel* PACS and SPIRE instruments. We show that the water lines can probe shock dynamics and chemistry, and discuss the physical conditions of water and CO emission.

### 2. OBSERVATIONS

We performed *Herschel* HIFI and PACS observations towards the molecular supernova remnant G349.7+0.2 on board of the *Herschel* Space Observatory. The spectra have been reduced using recent version of *Herschel* Interactive Processing Environment (HIPE) version

<sup>1</sup> SETI Institute, 189 N. Bernardo Ave, Mountain View, CA 94043; jrho@seti.org

<sup>2</sup> NASA Ames Research Center, MS 211-1, Moffett Field, CA 94043

<sup>3</sup> CRESST/University of Maryland, Baltimore County, Baltimore, MD 21250 and NASA Goddard Space Flight Center, Greenbelt, MD 20771, USA; john.w.hewitt@nasa.gov

<sup>4</sup> SOFIA Science Center, NASA Ames Research Center, MS 211-1, Moffett Field, CA 94035; aboogert@sofia.usra.edu

<sup>5</sup> Department of Physics & Astronomy, San Jose State University, San Jose, CA 95192-0106; michael.kaufman@sjsu.edu

<sup>6</sup> LERMA, UMR 8112 du CNRS, Observatoire de Paris, École Normale Supérieure, 24 rue Lhomond, 75231 Paris Cedex 05, France; antoine.gusdorf@lra.ens.fr

12.1. HIFI observations of H<sub>2</sub>O were conducted on 2012 September 29 (obsid=1342251666) and 2012 September 22 (obsid= 1342251494) in pointing mode with a position switch (offset of -3' in RA and 3' in Dec) towards 17<sup>h</sup>18<sup>m</sup>00.50<sup>s</sup> and Dec. -37°26'35" (J2000). Integration times were 915 s in Band 1a (557 GHz), and 1936 s in Band 4a (1113 GHz). The spectral resolutions are 1.10 MHz and 0.25 MHz for HIFI WBS and HRS, respectively. Figure 1 shows the field of view (FOV) of the PACS and HIFI instruments. The ground state ortho-water line,  $1_{10}$ - $1_{01}$  transition, at 557 GHz was detected, as shown in Figure 2, while no line was detected at the frequency of the para-H<sub>2</sub>O line at 1113 GHz. We examined the off-position spectra at 557 GHz and concluded that the position is clean and does not contaminate the observed emission. The main beam efficiencies were corrected based on the release note of new beam efficiency measured on Mars<sup>7</sup> which results in 22% increase in the line brightnesses for 557 GHz line compared to that using Roelfsema et al (2012). The beam sizes of the 557 and 1113 GHz water line observations are 44" and 19", respectively. We have used spectral settings that avoid spurs in Bands 1a and 4a.

PACS spectral observations took place on 2012 October 5 for 3,498 s (obsid = 1342252274), and covered from 72.2 to 90.76  $\mu$ m and from 112.2 to 181.4  $\mu$ m. The pointed observation was made in chopping/nodding Mode with medium chopping throw. The PACS FOV is overlapped with the HIFI FOV except for one pixel on the top right where an ultra-compact HII region (UC HII) is present (see Fig. 1a). This pixel corresponds to the brightest pixel on the PACS continuum map. We extracted PACS spectra at the same region covered by HIFI which excluded the brightest pixel. The PACS observations yielded a 5×5 grid map with a pixel size of 9.4"×9.4". The spectral resolution ranges from 1000 at 200  $\mu$ m to 5000 at 51 $\mu$ m. SPIRE FTS observations took place on 2012 September 24 for 3,003 s (obsid = 1342251325). The beam size of the SPIRE SSW and SLW are 17-21" and 29"-42", respectively.

### 3. BROAD WATER LINE WITH HIFI

Figure 2 shows the broad 557 GHz water line observed towards the SNR G349.7+0.2. The red branch shows prominent wings with a smooth Gaussian profile while the blue branch does not and instead features some dips in the wings which are likely absorption lines in the line of sight. We have fit the spectrum with Gaussian lines and Table 1 summarizes the widths (FWHM) of velocity ( $\Delta V$ ), the velocity at center ( $V_o$ ), the integrated intensity and the surface brightness (in  $nWm^{-2}sr^{-1} = 10^{-9}Wm^{-2}sr^{-1}$ ). The spectrum can be reproduced by three kinematic components with widths of 144, 27 and 4  $km s^{-1}$ . respectively; we refer to them as extremely broad, broad and narrow water lines (EBWL, BWL, and NWL). G349.7+0.2 is the only SNR which reveals this extremely broad (144  $km s^{-1}$ ) component among the molecular cloud interacting SNRs we observed with Herschel. The LSR velocity of G349.7+0.2 is 16  $km s^{-1}$  (Dubner et al. 2004) and the velocity shifts of the three components are red-shifted at +18, +3, and +1.4

$km s^{-1}$  for EBWL, BWL, and NWL, respectively. This water line exhibits shock dynamics revealed by water.

The X-ray temperature observed for G349.7+0.2 is 0.7- $1 \times 10^7 K$  (Lazendic et al. 2005), which implies a shock velocity of 760  $km s^{-1}$ . When assuming pressure equilibrium between the inter-cloud medium (ICM) and clouds, and assuming a ICM density ( $n_{ICM}$ ) of  $\sim 5$ -10  $cm^{-3}$  from X-ray gas (Lazendic et al. 2005; Chevalier 1999), the shock velocity in the cloud ( $V_{sc} = \sqrt{(n_o/n_c)} \times V_s$ ) is approximately 55-76 and 17-24  $km s^{-1}$  for  $n_c$  of  $10^3$  and  $10^4 cm^{-3}$ , respectively. The observed velocity of 144  $km s^{-1}$  is much higher than the expected shock velocity in a cloud when a pressure equilibrium is assumed.

The velocity component of 144  $km s^{-1}$  is due to strong supernova shocks and the broadest water line detected to date in the literature. This may be compared with widths of 81  $km s^{-1}$  (Mottram et al. 2015), 50  $km s^{-1}$  (Leurini et al. 2014), 30  $km s^{-1}$  (Melnick et al. 2010) and 20  $km s^{-1}$  (Kama et al. 2013) from low-mass protostars, high-mass star-forming regions, and objects towards Orion and OMC-2 FIR 4, respectively. Similar widths ( $\sim 50$ -60  $km s^{-1}$ ) are associated with high velocity water bullets in low-mass protostars (Kristensen et al. 2011). The EBW emission could arise from the high-velocity shell structure seen in the H<sub>2</sub> emission with components covering the velocity range -40  $km s^{-1}$  to +40  $km s^{-1}$  (Lazendic et al. 2010), while a similar structure could be giving rise to the broad water emission.

The HIFI water spectrum of G349.7+0.2 shows another interesting feature, different from other SNRs (e.g. S05) or astronomical objects: a narrow (FWHM=3.7  $km/s$ ) emission line (the NWL component). Narrow water lines are seen toward low mass (Kristensen et al. 2012) and high-mass YSOs (Marseille et al. 2010). They often have P Cygni and reversed P Cygni profiles, originating from envelope expansion and infall, respectively. In some cases only narrow emission lines are observed, in particular for YSOs associated with PDRs (Kristensen et al. 2012), and this gas may have been released from ices by photodesorption. For G349.7+0.2, the existence of ices along the line of sight is expected following the extinction of  $A_v = 30$  mag, high densities and temperatures below the sublimation temperature of  $\sim 100$  K. This indicates there is a source of non-thermal desorption, particularly due to photodesorption (Hollenbach et al. 2009; Caselli et al. 2012; Caselli & Ceccarelli 2012). The NWL might trace sublimation or photodesorption of the ices near the UC HII region, although it is presently unclear if the UC HII region is associated with the SNR, or if its location is related to the dense cloud which interacts with the SNR. Alternately, a strong cosmic ray flux or a secondary FUV field generated by the cosmic ray destruction of H<sub>2</sub> might photodesorb H<sub>2</sub>O, but in this case a strongly enhanced cosmic ray flux would be needed, considering that the observed NWL is ten times stronger than that observed in the dense core L1544 (Caselli et al. 2012).

More likely, however, shocks may have released H<sub>2</sub>O into the gas phase. The narrow component of CO showed blue- or red-shifted emission and the central velocity differs at different positions; the CO gas is suggested to have shocked origin (Dubner et al. 2004). The fact that the velocity of NWL is consistent with the CO indicates

<sup>7</sup> <http://herschel.esac.esa.int>

that they are from the same gas. We suggest that the NWL is likely shocked gas from denser clumps or reformed molecules behind a dissociative shock (see Section 5 for details). Further observational evidence would be needed to determine the origin of the NWL. The BWL component with FWHM of  $27 \text{ km s}^{-1}$  is comparable to those in IC 443 observed by Snell et al. (2005). The width of the component is consistent with the C-shock that is responsible for  $\text{H}_2$  emission (Hewitt et al. 2009).

#### 4. MOLECULAR AND FINE-STRUCTURE LINES WITH PACS AND SPIRE

The  $\text{H}_2\text{O}$ , CO, [OI] and [CII] lines detected using PACS and SPIRE are listed in Table 2. The  $\text{H}_2\text{O}$  lines detected with PACS are shown in Figure 3. (We also detected OH lines; these will be discussed in a future paper.) Using the PACS cube, we produced three line maps of  $\text{H}_2\text{O}$ , CO and [O I]. The spatial distribution of the  $\text{H}_2\text{O}$  and [O I] lines are shown in Figure 1.  $\text{H}_2\text{O}$  emission is strongest at the southern shell of the SNR, while [O I] is strongest toward the SNR central position. CO lines from  $J_{\text{upper}}=4$  to 13 were detected with SPIRE, and most CO lines from  $J_{\text{upper}}=16$  to 36 were detected with PACS. Detected ortho- $\text{H}_2\text{O}$  lines are seen at 1670 (179.6), 1717 (174.7), 2640 (113.6) GHz ( $\mu\text{m}$ ). All ortho-water lines that are within our wavelength range were detected, except 1097 GHz (273.475  $\mu\text{m}$ ) for which we only note a hint of emission in the SPIRE data. The CO map (not shown) is very similar to the  $\text{H}_2\text{O}$  map, and the  $\text{H}_2\text{O}$  map is globally similar to the [O I] map. The  $\text{H}_2\text{O}$  peak is between the two bright peaks of the PACS 70  $\mu\text{m}$  map, while the peak [O I] emission is close to the left bright peak of the PACS 70  $\mu\text{m}$  map. None of the para- $\text{H}_2\text{O}$  lines were detected including the ground state para- $\text{H}_2\text{O}$   $1_{11}\text{-}0_{00}$  line at 1113 GHz observed with HIFI. The upper limit of the 1113 GHz line is  $0.06 \text{ nWm}^{-2} \text{ sr}^{-1}$ , which is a factor of 15 fainter than the sensitivity of 557 GHz line.

#### 5. DISCUSSION

In order to understand the physical conditions in the shocked gas, we begin by constructing an excitation diagram for the observed CO lines. A two-temperature fit yields a low temperature ( $T_{\text{low}}$ ) of 170 K with a column density ( $N_{\text{low}}$ ) of  $1 \times 10^{16} \text{ cm}^{-2}$ , and a high temperature ( $T_{\text{high}}$ ) of 560 K with ( $N_{\text{high}}$ ) of  $1 \times 10^{15} \text{ cm}^{-2}$ . These may be compared with the two-temperature LTE fit of  $\text{H}_2$  emission observed with *Spitzer* by Hewitt et al. (2009) who have found a warm component of  $N(\text{H}_2)_{\text{warm}} = 2.8 \times 10^{20} \text{ cm}^{-2}$ , and  $T_{\text{warm}} = 467 \text{ K}$  and  $\text{OPR}_{\text{warm}} = 1$ , and  $N(\text{H}_2)_{\text{hot}} = 5.2 \times 10^{18} \text{ cm}^{-2}$ , and  $T_{\text{hot}} = 1647 \text{ K}$ . Comparing the CO and  $\text{H}_2$  column densities in the two components gives CO abundances  $x(\text{CO}) \sim 3 \times 10^{-5} - 2 \times 10^{-4}$ . The CO rotational diagram as a function of  $J_{\text{upper}}$  are shown in Figure 5. The surface brightness of CO peaks at approximately  $J_{\text{upper}}$  of 15.

We may compute the column density of ortho- $\text{H}_2\text{O}$  following the procedure outlined by Snell et al. (2005, see Eq. 1:  $N_{\text{H}_2\text{O}} \propto \int T dv$ ) for water in the low-excitation limit ( $n \ll n_{\text{crit}}$ ). Using an assumed gas density of  $5 \times 10^5 \text{ cm}^{-3}$  yields water columns of  $6.0 \times 10^{13}$ ,  $2.0 \times 10^{13}$  and  $3.6 \times 10^{12} \text{ cm}^{-2}$  in the EBWL, BWL and NWL components, respectively. An excitation diagram of the four observed water lines is shown in Figure 4. For  $\text{H}_2\text{O}$

TABLE 1  
GAUSSIAN VELOCITY COMPONENTS OF HIFI WATER LINE AT 557 GHz

$\Delta V$ (km/s)	$V_o$ (km/s)	$\int T dv$ (K km/s)	Surf. Brightness ( $\text{nWm}^{-2} \text{ sr}^{-1}$ )
$3.7 \pm 0.20$	$17.44 \pm 0.07$	0.53	0.17
$27.1 \pm 0.90$	$19.00 \pm 0.27$	2.95	0.98
$144.0 \pm 3.9$	$33.89 \pm 1.49$	8.82	3.30

TABLE 2  
FLUXES OF PACS-DETECTED  $\text{H}_2\text{O}$  AND CO LINES

Species Transition	Frequency in GHz (Wavelength in $\mu\text{m}$ )	E(up) (K)	S.B. ( $\text{nWm}^{-2} \text{ sr}^{-1}$ )
o- $\text{H}_2\text{O}$ 2 <sub>12</sub> -1 <sub>01</sub>	1669.90 (179.65)	114.3	18.020
o- $\text{H}_2\text{O}$ 3 <sub>03</sub> -2 <sub>12</sub>	1716.77 (174.74)	196.7	14.335
o- $\text{H}_2\text{O}$ 4 <sub>14</sub> -3 <sub>03</sub>	2640.47 (113.61)	323.4	39.543
CO (4-3)	461.04 (650.70)	55.3	7.503
CO (5-4)	576.26 (520.59)	82.9	12.35
CO (6-5)	691.47 (433.85)	116.1	19.42
CO (7-6)	806.65 (371.90)	154.8	29.74
CO (8-7)	921.80 (325.45)	199.1	41.56
CO (9-8)	1036.91 (289.32)	248.8	41.31
CO (10-9)	1151.99 (260.42)	304.1	47.87
CO (11-10)	1267.01 (236.77)	364.9	47.87
CO (12-11)	1382.00 (217.07)	431.3	51.86
CO (13-12)	1496.92 (200.41)	503.1	48.79
CO (16-15)	1841.35 (162.92)	751.7	53.13
CO (18-17)	2070.68 (144.88)	944.9	45.53
CO (22-21)	2528.17 (118.66)	1397.4	32.62
CO (29-28)	3325.01 (90.225)	2399.8	9.713
CO (30-29)	3438.36 (87.250)	2564.8	15.29
CO (32-31)	3664.68 (81.862)	2911.2	12.26
CO (33-32)	3777.64 (79.414)	3092.5	5.614
CO (36-35)	4115.61 (72.893)	3668.8	9.595
[O I]	2061.04 (145.557)	188	500.9
[C II]	1901.58 (157.763)	92	735.6

molecular data<sup>8</sup>, we used Tennyson et al. (2001) for the energy levels, and Barber et al. (2006) for radiative transition rates, and Faure & Josselin (2008) for collision rates. The analysis of the excitation diagram gives similar total  $\text{H}_2\text{O}$  columns of a few  $\times 10^{13} \text{ cm}^{-2}$  obtained from the low temperature component. We do not know which of the  $\text{H}_2$  temperature components the  $\text{H}_2\text{O}$  emission corresponds to, but the resulting water abundances range from  $\sim 10^{-8}$  to  $\sim 10^{-5}$  with respect to warm and hot  $\text{H}_2$ , respectively. We note that the column densities derived above are inversely proportional to the assumed gas density and thus should be interpreted with some caution.

We compare the  $\text{H}_2\text{O}$ , CO and  $\text{H}_2$  brightnesses with shock models. Bright  $\text{H}_2$  emission was detected with the *Spitzer* IRS, and Hewitt et al. (2009) showed two possible scenarios of shock models based on  $\text{H}_2$  emission. Their best-fit model is a combination of two C-shock models, one with a pre-shock density  $n_0 = 10^6 \text{ cm}^{-3}$  and a shock velocity  $V_s = 10 \text{ km s}^{-1}$ , and the other with  $n_0 = 10^5 \text{ cm}^{-3}$  with  $V_s = 40 \text{ km s}^{-1}$ . The associated filling factors ( $\Phi$  or FF) are 0.61 and 0.007, respectively. The second best model is a combination of a C-shock (with a density of  $n_0 = 10^6 \text{ cm}^{-3}$  and  $V_s = 10 \text{ km s}^{-1}$ ) and a J-shock (with a  $n_0 = 10^4 \text{ cm}^{-3}$  and  $V_s = 110 \text{ km s}^{-1}$ ). First, we tried the C-shock model following

<sup>8</sup> see <http://home.strw.leidenuniv.nl/~moldata/H2O.html>



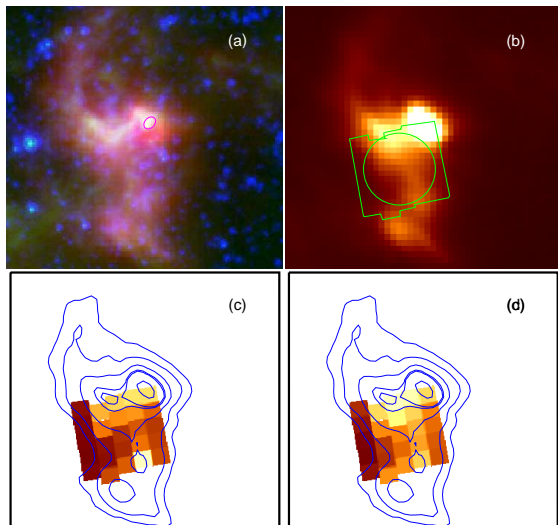


FIG. 1.— *Herschel* and *Spitzer* images of G347.9+0.2. (a) *Spitzer* three color images (blue, green and red represents 4.5, 8 and 24  $\mu\text{m}$ , respectively). MM(1) source which is a possible UC HII region (see Lazendic et al. 2010) is marked as an ellipse in red. (b) *Herschel* PACS broad band at 70  $\mu\text{m}$  where the brightest peak (right side) is MM(1) source and the second strongest peak (left side) is center of the SNR. The FOVs of HIFI (a circle: 557 GHz line) and PACS (a square) are marked. (c) Water map at 113  $\mu\text{m}$  (c) and (d) [O I] map at 145  $\mu\text{m}$  generated by PACS spectral cube. The contours are from the PACS 70  $\mu\text{m}$  map. The contour levels correspond to 0.24, 0.37, 0.72, 1.84, 1.96 and 5.54 Jy/(3.2''x3.2'' pixel). The maps have 3 arcmin FOV centered on 17<sup>h</sup>18<sup>m</sup>00<sup>s</sup> and Dec. -37°26'20.93'' (J2000).

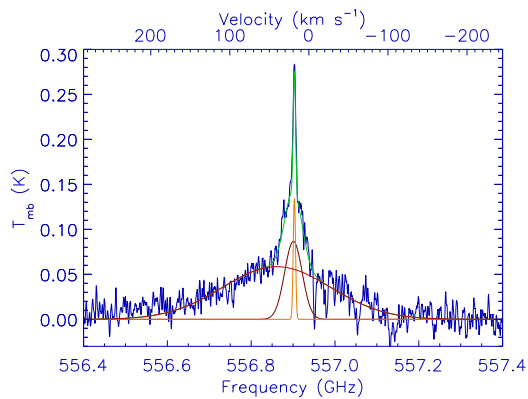


FIG. 2.— *Herschel* HIFI spectrum of G349.7+0.2 shows a broad water line at 557 GHz. The gaussian fits (total fit is marked in green) reveal the width of three kinematic components of 144 (in red), 27 (in brown) and 4 (in orange) km s<sup>-1</sup>.

the method presented in Gusdorf et al. (2008, 2012) to compare the CO data with shock models. This model solves the magneto-hydrodynamical equations in parallel with a large chemical network for stationary C- and J-type shocks (Flower et al. 2003) and combine the outputs with a radiative transfer module based on the LVG approximation. A combination of the two C-shock model that reproduced the H<sub>2</sub> emission with FF $\sim$ 1 (see Fig. 7 from Hewitt et al. 2009) can not re-produce either CO (Fig. 5 or 6) or H<sub>2</sub>O (Fig. 7). The same C-shock model using FF of 0.05 may reproduce high-J CO lines, but low-J lines don't match with the model. The same C-shock model could not produce the observed H<sub>2</sub>O lines with an assumption of FF=1; however, it does reasonably match

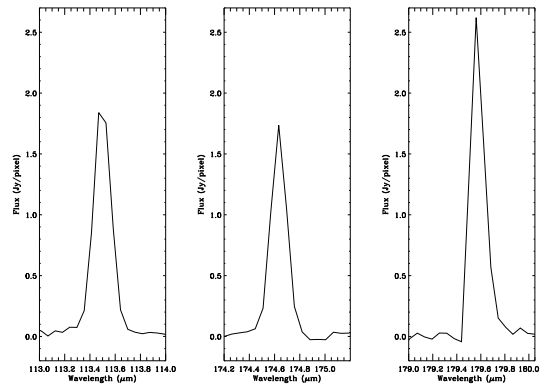


FIG. 3.— Three *Herschel* PACS water spectra of G349.7+0.2. The lines are unresolved.

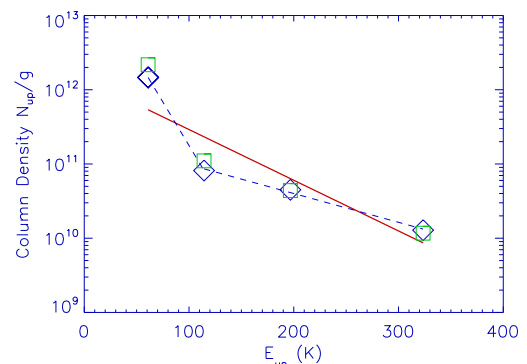


FIG. 4.— Water rotational diagram using the HIFI ( $E_{up}$  of 61 K using the intensity integrated over the whole velocity profile) and PACS data. Only ortho-H<sub>2</sub>O lines were detected. The one-temperature fit (in red) indicates  $N(\text{H}_2\text{O}) = 1.4 \times 10^{12} \text{ cm}^{-2}$  and a temperature of 68 K. The two-temperature LTE fit marked in blue yielded a low temperature ( $T_{low}$ ) of 18 K with a column density ( $N_{low}$ ) of  $4.0 \times 10^{13} \text{ cm}^{-2}$ , and a high temperature ( $T_{high}$ ) of 112 K with ( $N_{high}$ ) of  $2.3 \times 10^{11} \text{ cm}^{-2}$ . Non-LTE models ( $n=10^5 \text{ cm}^{-3}$  and  $N_{\text{H}_2\text{O}} = 3 \times 10^{13} \text{ cm}^{-2}$  with a range of kinetic temperature of 100 - 1000) are marked as squares in green.

the H<sub>2</sub>O lines with an assumption of FF=0.05 (see Fig. 7).

We find a J-shock model with a velocity of 80 -100 km s<sup>-1</sup> and a density of  $n_0 \sim 10^4 \text{ cm}^{-3}$  (HM89) provides a good fit to the CO rotational diagram (see Fig. 5), and is consistent with the EBWL flux. A direct comparison of the surface brightnesses of CO with the J-type shock models of HM89 (their Fig. 7) is shown in Figure 6. The total intensity of the observed water lines are 76.4 nW m<sup>-2</sup> sr<sup>-1</sup>, which is comparable to the predicted flux from the J-shock model with velocity of 80 -100 km s<sup>-1</sup> and a density of  $n_0 \sim 10^4 \text{ cm}^{-3}$  (see Fig. 9 of HM89). This J-shock model can also explain the fluxes of [O I] 145  $\mu\text{m}$  and [C II] 157  $\mu\text{m}$  observed with the *Herschel* PACS and [Ne II] and [Ne III] lines with *Spitzer* IRS. It is surprising that the same J-shock model can explain both CO and ionic lines, because *Spitzer* results show that the molecular (H<sub>2</sub>) lines segregate from ionic lines within the *Spitzer* IRS slits (H09). Based on *Spitzer* data, a principal component analysis of the spectral-line maps by Neufeld et al. (2007) also shows that molecular lines (H<sub>2</sub> J>2) belong different group from ionic lines and can be explained by different shock model from that

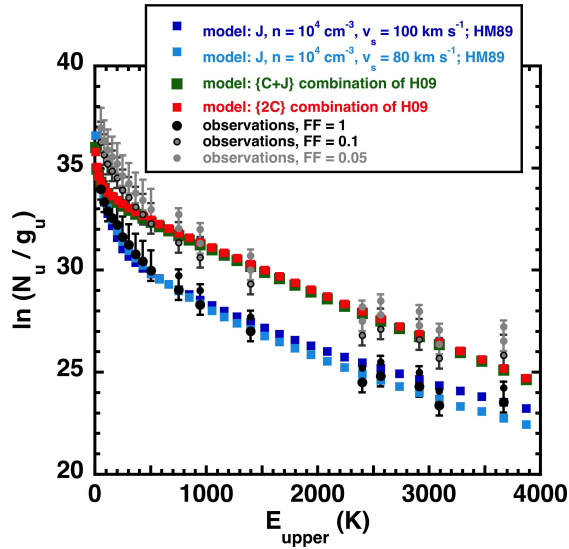


FIG. 5.— High- $J$  CO rotational diagram as a function of rotational level superposed on two C-shock model from Gusdorf et al. (2012) using the model parameters that produce  $H_2$  emission (Hewitt et al. 2009, H09), and J-shock model with a density of  $10^4 \text{ cm}^{-3}$  and a shock velocity of  $80 \text{ km s}^{-1}$  from Hollenbach & McKee (1989). ‘FF’ indicates the filling factor.

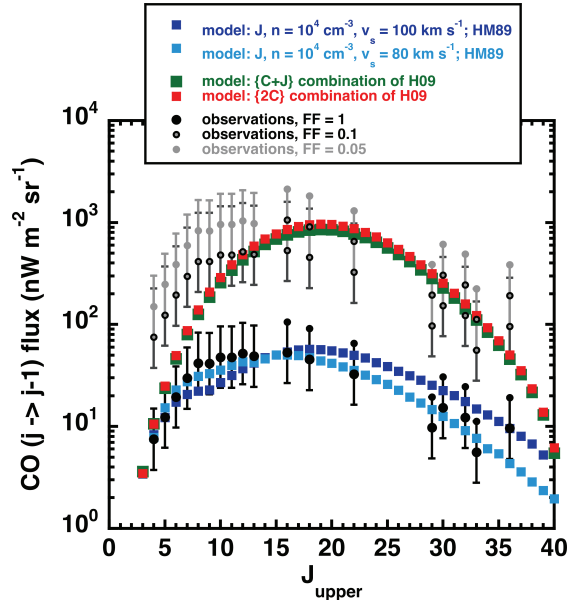


FIG. 6.— High- $J$  CO brightness diagram as a function of rotational level superposed on two C-shock model from Gusdorf et al. (2012) using the model parameters that produce  $H_2$  emission (Hewitt et al. 2009, H09), and J-shock model with a density of  $10^4 \text{ cm}^{-3}$  and a shock velocity of  $80 \text{ km s}^{-1}$  from Hollenbach & McKee (1989). ‘FF’ indicates a filling factor.

for ionic lines. If a blast wave with a velocity of  $80 \text{ km s}^{-1}$  moves into a dense clump, it would send a converging spherical shock into the clump. The blue- and red-shifted lines could be shocked clumps coming towards us or moving away from us with  $80 \text{ km s}^{-1}$  velocity, respectively; this causes a broad line as large as  $160 \text{ km s}^{-1}$ . In contrast, water emission in another molecular interacting SNR IC 443 shows the same width as those in CO,  $20 - 30 \text{ km s}^{-1}$ , which show the ambiguity between J-shock and C-shock models as discussed in Snell et al. (2005). The EBWL in G349.7+0.2 is a direct

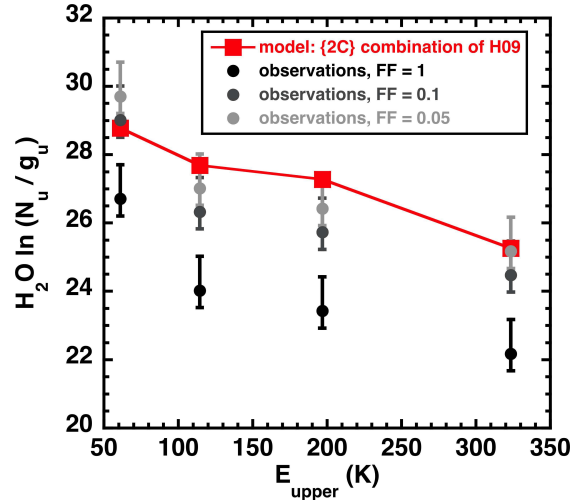


FIG. 7.—  $H_2O$  rotational diagram as a function of energy level for the same C-shock model as that in Figures 5 and 6.

evidence of high-velocity J-shocked material. The same J-shock could not produce the observed  $H_2$  brightnesses of G349.7+0.2. Hewitt et al. (2009) suggested that  $H_2$  emission is explained with the C-shock model.

The observed water gas may or may not be in LTE because these densities are much lower than the critical density of water ( $\sim 10^9 \text{ cm}^{-3}$ ). We have run grids of non-LTE RADEX (van der Tak et al. 2007) models for density varying from  $10^4$  to  $10^7 \text{ cm}^{-3}$  and column density of  $H_2O$  varying from  $3 \times 10^{11}$  to  $3 \times 10^{15} \text{ cm}^{-2}$  for temperature from 25 K to 500 K, with steps of 25 K. A water column density of  $10^{13} - 10^{14} \text{ cm}^{-2}$  and the inferred density of  $10^4 \text{ cm}^{-3} - 10^6 \text{ cm}^{-3}$  is consistent with the four water lines and the kinetic temperature is greater than the excitation temperature obtained from the LTE model (see Fig. 4). The predicted fluxes from non-LTE models with a column density of  $3 \times 10^{13} \text{ cm}^{-2}$  and a density of  $10^5 \text{ cm}^{-3}$  for a kinetic temperature range of 100 - 1000 K are also shown in Figure 4. The fluxes from the model are consistent with the observed line brightnesses. Even if the lines are thick, the transitions are effectively thin (see detailed discussion in S05) because the photons leak out by sequential absorption and re-radiation without collisional de-excitation.

We compared the abundances of  $H_2O/H_2$  and  $H_2O/CO$  using the water column density obtained from the non-LTE model described above. For a temperature of  $\sim 200 \text{ K}$ , the abundance of  $H_2O/H_2$  is approximately  $10^{-6} - 10^{-7}$  using non-LTE value of  $N(H_2O)$  of  $10^{13-14} \text{ cm}^{-2}$ ; the column density derived from LTE model could underestimate the abundance. The abundance of  $H_2O/CO$  is 0.1 - 0.003 for a range of temperature of 150-600 K. The abundances are comparable to those estimated for 3C391 using ISO (Reach & Rho 1998). There are two reasons that it is challenging to determine if our estimated abundance is low or high compared with shock models or other objects. We show a J-shock model with a high velocity ( $\sim 80 \text{ km s}^{-1}$ ) is consistent with the rotational diagram of CO emission and the total flux of water. (Detailed J-shock models of water lines with high shock velocities ( $> 50 \text{ km s}^{-1}$ ) are currently not available.) Most water abundance comparisons have been done with C-shock models (Kaufman & Neufeld 1996;

Flower & Pineau Des Forêts 2010). Moreover, our water lines show three components (VBL, BL and NL) while we don't have resolved CO lines. For our analysis we assume that all PACS lines have the same profiles as that of the HIFI water line. The resolved CO line is required to accurately estimate the H<sub>2</sub>O/CO abundance since the portion of VBL, BL and NL to the total may be different. One would need to estimate the abundance for each of VBL, BL and NL, respectively. Behind a J-shock, the abundance of water rises due to the rapid neutral-neutral reactions; later, H<sub>2</sub>O can freeze out. Perhaps it is possible that water in EBWL has a higher abundance than those of NL or BL components.

The extremely broad water line could be simply from short-lived molecules formed in high velocity J-shocks which have not had time to freeze out. However, it may be from more complicated geometry such as high-velocity water bullets or an expanding shell in high-velocity. Fu-

ture observations of velocity-resolved CO, H<sub>2</sub>O, OH and H<sub>2</sub> would be crucial to advance our understanding of oxygen chemistry of neutral-neutral and/or ion-neutral reactions in the process of converting oxygen to H<sub>2</sub>O.

Support for this work, part of the NASA Herschel Science Center (through JPL/Caltech), Astrophysics Data Analysis Program (grant NNX12AG97G) and Theoretical Research/Laboratory Astrophysics Program was provided by NASA. We thank David Hollenbach for insightful and critical comments which helped to significantly improve the paper. We thank Tom Pannuti for discussion on SNRs, Herschel Science Center staff members including Ivan Valtchanov, David Teyssier, and David Shupe for their support on data reduction, and calibration, and Emmanuel Caux for various discussion on and updating CASSIS.

#### REFERENCES

- Andersen, M., Rho, J., Reach, W. T., Hewitt, J. W., & Bernard, J. P., 2011, *ApJ*, 742, 7
- Anderl, S., Gusdorf, A., & Güsten, R., 2014, *A&A*, 569, 81
- Archer, P. D. et al., 2014, *Journal of Geophysical Research (JGRE)*, 119, 237
- Barber, R. J., Tennyson, J., Harris, G. J., & Tolchenov, R. N., 2006, *MNRAS*, 368, 1087
- Caselli, P. et al., 2012a, *ApJ*, 759, 37
- Caselli, P. & Ceccarelli, C., 2012b, *ARA&A*, 20, 56
- Chevalier, R. A., 1999, 511, 798
- Dubner, G., Giacani, E., Reynoso, E., Parón, S., 2004, *A&A*, 426, 201
- Faure, A. & Josselin, E., 2008, *A&A*, 492, 257
- Flower, D. R. & Pineau Des Forêts G., 2010, *MNRAS*, 406, 1745
- Frail, D. A. et al. 1996, *AJ*, 111, 1651
- Gusdorf, A. et al., 2012, *A&*, 542, 19
- Hewitt, J. W., Yusef-Zadeh, F., Wardle, M., 2008, *ApJ*, 683, 189
- Hewitt, J. W., Rho, J., Andersen, M., & Reach, W. T., 2009, *ApJ*, 694, 126 (H09)
- Hollenbach, D. & McKee, C. F., *ApJ*, 1989, 342, 306 (HM89)
- Hollenbach, D., Kaufman, M.J, Bergin, E. A., & Melnick, G.J., 2009, *ApJ*, 690, 1497
- Kama, M. et al., 2013, *A&A*, 556, 57
- Karska A. et al., 2014, *A&*, 572, A9
- Kaufman, M.J, & Neufeld, D. A. 1996, *ApJ*, 456, 611
- Kristensen et al. 2010, *A&* 521, L30
- Kristensen et al. 2010, *A&* 531, L1
- Kristensen et al. 2012, *A&* 542, 8
- Lazendic, J. S. et al., 2005, 618, 734
- Lazendic, J. S., Wardle, M., Whiteoak, J.B., Burton, M. G., & Green, A.J., 2010, *MNRAS*, 409, 371
- Leurini et al., 2014, *A&A*, 564, 111
- Marseille, M.G. et al. 2010, *A&A*, 521, L32
- Mottram, J. C., et al., 2015, *A&A*, 574, 3
- Melnick, G. J. et al., 2010, *A&A*, 521, L27
- Neufeld, D. A. et al., 2007, *ApJ*, 664, 890
- Neufeld, D. A., Gusdorf, A., Güsten, Rolf; Herczeg, G. J., Kristensen, L., Melnick, Gary, J., Nisini, B., Ossenkopf, V., Tafalla, M., van Dishoeck, E., 2014 781, 102
- Reach, W.T., and Rho, J., 1996, *A&A*, 315, 277
- Reach, W.T., and Rho, J., 1998, *ApJ*, 507, 93L
- Reach, W.T., Rho, J. & Jarrett, T. H., 2005, *ApJ*, 618, 297
- Reach, W. T., Rho, J., Tappe, A., Pannuti, T. G., Brogan, C. L., Churchwell, E. B., Meade, M. R., Babler, B., Indebetouw, R., & Whitney, B. A. 2006, *AJ*, 131, 1479
- Rho, J. & Petre, R., 1998, *ApJ*, 503, L167
- Roelfsema, P.R. et al., 2012, *A&A*, 537, 17
- Santangelo, G. et al., 2014, *A&A*, 2014, 569, L8
- Snell, R.L., Hollenbach, D., Howe, J.E., Neufeld, D. A., Kaufman, J.J., Melnick, G.J., 2005, *ApJ*, 620, 758 (S05)
- Tennyson, J., Zobov, N.F., Williamson, R., Polyansky, O. L., & Bemath, P. F., P2001, *J. Phys. Chem. Ref. Data*, 30, 735
- Tian, W.W. & Leahy, D. A., 783, 2
- van Dishoeck, E. F., Jansen, D.J, & Phillips, T.G., 1993, *A&A*, 279, 541
- van Dishoeck, E. F. et al., 2011, *PASP*, 123, 138
- van der Tak, F.F.S., Black, J. H. Schöier, F.L, Jansen, D.J., van Dishoeck, E. F., *A&A*, 468, 627
- Yamauchi, S., Koyama, K., Kinugasa, K., Torii, K., Nishiuchi, M., Kosuga, T., Kamata, Y., 1998, *Astron. Nachr*, 319,111